Microwave-assisted *in situ* laser dye incorporation into high sensitivity whispering gallery mode microresonators

OPEN ACCESS
IOP Publishing
Journal of Physics D: Applied Physics
J. Phys. D: Appl. Phys. **55** (2022) 055101 (10pp)
https://doi.org/10.1088/1361-6463/ac2e34

Microwave-assisted *in situ* laser dye incorporation into high sensitivity whispering gallery mode microresonators

Jesús S Mondragón-Ochoa[1,7], José González-Rivera[2,3,7], Cigdem Toparli[1,8], Rizwana Khanum[4], Rakesh S Moirangthem[4], Celia Duce[2], Carlo Ferrari[5,*], Giuseppe Barillaro[3] and Andreas Erbe[1,6,*]

[1] Max-Planck-Institut für Eisenforschung GmbH, Max-Planck-Str. 1, 40237 Düsseldorf, Germany
[2] Department of Chemistry and Industrial Chemistry, University of Pisa, Via G. Moruzzi 3, 56124 Pisa, Italy
[3] Dipartimento di Ingegneria dell'Informazione, Università di Pisa, Via G. Caruso 16, 56122 Pisa, Italy
[4] Nanophotonics Lab, Department of Physics, Indian Institute of Technology (Indian School of Mines), Dhanbad, Jharkhand 826004, India
[5] National Research Council of Italy (C.N.R.), National Institute of Optics, (INO)—UOS Pisa, Via G. Moruzzi 1, 56124 Pisa, Italy
[6] Department of Materials Science and Engineering, NTNU, Norwegian University of Science and Technology, 7491 Trondheim, Norway

E-mail: carlo.ferrari@ino.cnr.it and WGM-microlasers@the-passivists.org

Received 15 July 2021, revised 5 October 2021
Accepted for publication 8 October 2021
Published 26 October 2021

Abstract

Optical whispering gallery mode microresonators (WGM-μRs) are powerful sensitive components with many analytical applications. Here, spherical WGM-μRs have been synthesised in a single-step microwave (MW)-assisted heterophase polymerisation. The microresonators are based on poly(styrene) beads into which the organic lasing dye nile red was incorporated as gain medium *in situ* during the polymerisation. The particle diameter and diameter distribution of the synthesised particles were tuned in the range of around 200 nm up to 50 μm by adjusting the concentration between stabiliser poly-(*N*-vinyl pyrrolidone) (PVP) and monomer styrene, and the solvent composition in the dispersion process. Lower water content enabled the synthesis of spherical particles with large size polydispersity, from which WGM-μRs with a variety of diameters were selected. Microspheres with diameters $\gtrsim$3.5 μm supported WGMs. The WGMs were excited through free space via the fluorescence of the laser dye. Pumping power levels $<$1 μW were sufficient to excite WGMs. WGM shifts of beads with diameter between $\approx$5 and 30 μm measured in air and water show a sensitivity up to 54 nm/RIU for the smallest particles. Dye doped WGM-μR in the low μm size range obtained by the

[7] These authors contributed equally.
[8] Present address: Middle East Technical University, Department of Metallurgical and Materials Engineering, Ankara, Turkey.
[*] Authors to whom any correspondence should be addressed.

MW-assisted polymerisation process with its versatility, low processing times and high yields opens new horizons for the applications of these systems as sensors.

Supplementary material for this article is available online

Keywords: whispering gallery mode, morphology-dependent resonances, laser, polymerisation, microwave, refractive index sensing

(Some figures may appear in colour only in the online journal)

1. Introduction

Optical microresonators are highly sensitive to the surrounding environment. Changes of physical properties such as temperature [1, 2], humidity [3], electric field strength [4], or others [5, 6] can be detected via changes in the refractive index on a variety of materials such as polymers, metal oxides or other semiconductors [7–15]. Also nanoparticle decorated resonators have been realised, exploiting plasmonic coupling [16]. This sensitivity also opens up opportunities in biosensing [17], or for detection of individual nanoparticles [18]. Combination with comprehensive data processing strategies yielded uniquely identifiable spectral signatures [19], or local temperature measurements [1].

Whispering gallery mode microresonators (WGM-μRs) achieve superior optical cavities with a small mode volume and a high quality factor Q,

$$Q = \frac{\lambda}{\Delta\lambda}, \tag{1}$$

where $\Delta\lambda$ is the full width at half maximum (FWHM) of the resonance peak occurring at λ [20]. WGM-μRs can be obtained with various geometries, such as spheres, toroids, disks, rings, cylinders and capillaries [7, 8, 20]. Inclusion of laser dyes, e.g. into polymer-based WGM-μRs, yields microlasers with versatile chemical properties [8, 21, 22]. Polymer-based WGM resonators can be integrated into chip-based sensing platforms [23]. Sensitivity to environmental changes of lasing WGM-μRs can under certain conditions be lower than of their non-lasing counterparts [24]. Local temperature control was used to sensitively control laser emission from WGM-μRs [25]. A polymeric carrier may also act as protecting material that prevents lasing dye degradation [26].

The sensitivity S of a WGM-μRs sensor to the surrounding medium,

$$S = \delta\lambda/\delta n_e, \tag{2}$$

where δn_e denotes a change in the refractive index n_e of the surrounding medium, increases inversely with the particle diameter D [27], whereas Q decreases [7, 28]. Thus, particles with small D, and therefore low Q, are potentially promising for designing resonators with high sensitivity. While low-Q resonators have important applications for sensing inside the resonator [29], polymer microspheres combined with a gain medium, like an organic dye, are attractive to excite WGMs in suitable orders of Q [21]. Despite of several advantages that polymeric based WGM-μR lasers offer, their use as resonators has been reported in literature for sizes $\geqslant$10 μm [21]. Obviously, there must be a lower limit below which the resonator does not support WGMs any more, but near this limit, high sensitivity to the surrounding environment is expected. It is thus reasonable to exploit WGM-μR at lower diameters.

Simple approaches to prepare 10 s to 100 s of μm sized WGM-based microlasers include protein self assembly [30, 31], use of metal organic frameworks [32], and electrospinning [33, 34].

Approaches to synthesise polymer-based WGM-μRs involve typically several steps: (1) synthesis of polymeric microspheres, (2) loading, e.g. by swelling, of the gain media into the polymeric matrix, and (3) solvent evaporation and dye-doped microspheres purification [10, 13]. On the other hand, integrated polymerisation processes exist where a dye is directly loaded during the polymerisation, e.g. by dispersion polymerisation [35], or double emulsion polymerisation [36]. Both techniques have been applied to the synthesis of polymer particles with diameters ranging from nm to 100 s of μm [35]. In general, one-step approaches reduce the number of synthesis steps, but may be time consuming and have challenges with control of particle size and size distribution due to complex dye-monomer-surfactant-solvent interactions. A particular challenge for WGM-μRs is the need to prepare particles with sufficient quality in shape over a large, ideally very broad size range.

Microwave (MW) assisted dispersion polymerisation is an attractive method because it significantly reduces the processing time, energy consumption and equipment size compared to conventional methods [37–39]. Higher rates of polymerisation, narrow polymer polydispersity, greater yields, or even completely new reactions, have been reported for MW synthetic approaches [37, 40–46]. MW-assisted polymerisation of styrene has been reported with 60 min reaction times in MW oven-type devices [42, 43]. A novel scalable methodology based on coaxial MW technology inside standard laboratory equipment is used here for the synthesis optical microresonators based on polymer microspheres incorporating a laser dye. This configuration has been successfully used in several MW assisted chemical processes such as heterogeneous catalytic processes [47], nanoparticle syntheses [48, 49], and mesoporous materials syntheses [50]. In this configuration, MW irradiation ensures a selective homogeneous heating of the reaction mixture.

In this work, MW-assisted free radical polymerisation has been investigated for the preparation of spherical WGM-μRs

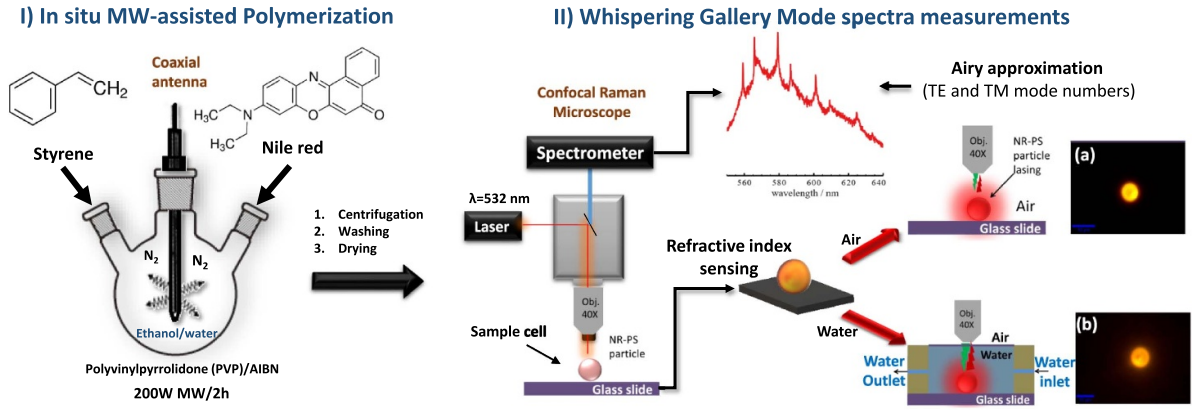

Figure 1. (I) Schematic representation of the set up for the synthesis of NR doped PS particles by *in situ* MW assisted polymerisation. (II) Principle of WGM measurements. Fluorescence images of a single, excited particle on a glass substrate in air (a) and in water (b).

based on poly(styrene) (PS). The organic lasing dye nile red (NR) has been incorporated into the PS as gain medium. PS with incorporated NR is referred to as PS-NR throughout this work. The kinetics of the polymerisation has been investigated gravimetrically, and the resulting particles have been characterised. Single particles have subsequently been investigated as WGM-μRs by excitation of the laser dye through free space. The setup and overall methodological approach is shown in figure 1. Full experimental information is available in the supplementary material (SM) (available online at stacks.iop.org/JPD/55/055101/mmedia).

2. Results and discussion

2.1. Synthesis of polymeric WGM-μ*Rs by* in situ *dye encapsulation through MW assisted polymerisation*

PS particles where synthesised through the coaxial MW assisted polymerisation process starting with the best conditions reported in literature [42, 43, 51–53] (SM-table 1). Figure 2 shows images and diameter distribution of several samples. Sample information is compiled in table 1. The PS particles of PS-0 showed a well-defined spherical shape with a bimodal size distribution (figure 2(c)). The size distribution peaks at $\langle D\rangle_{\text{low}} = (300 \pm 60)$ nm and $\langle D\rangle_{\text{high}} = (800 \pm 70)$ nm.

The introduction of NR into the PS particles by MW assisted polymerisation was firstly investigated by performing styrene polymerisation under the same reaction conditions as pure PS sample (PS-0 in table 1), but with the addition of NR (sample PS-NR-1 in table 1). Well defined spherical particles with $\langle D\rangle = (480 \pm 30)$ nm and a narrow size distribution were obtained (figures 2(d)–(f)). The introduction of NR thus did not have any adverse effects on the polymerisation reaction or the morphology obtained. Strong fluorescent emission of the PS-NR-1 particles was observed by fluorescence microscopy (figure 2(e-I)), showing the incorporation of NR.

The differences observed in diameter distributions between NR-free and NR-containing PS particles prepared at otherwise identical conditions may be related to a solvation effect, because of the similar chemical behaviour of NR and styrene. Accordingly to the literature [39, 43], we hypothesise that in the absence of NR, styrene is rapidly polymerised to small oligomers that continue to grow until the formation of the first polymeric particles. Styrene is continuously absorbed or trapped into the non-polar polymeric particles with a broad size distribution; the particles are stabilised by the PVP on their surface. Because of the loss of styrene, the reaction media became more and more polar. Rapidly, a complete consumption of styrene occurs. The smaller particles are hindered to grow leading to a bimodal diameter distribution. The introduction of NR during the polymerisation reaction may have caused NR-styrene interactions, promoting changes in the polarity of the reaction media throughout the entire polymerisation process. Styrene-NR form a hydrophobic, homogeneous and non-polar phase that promotes a slower and controlled styrene supply to growing particles thus resulting in a monomodal diameter distribution. The nucleation stage during dispersion polymerisation of styrene is well known to be a short-lived, critical, complex and very sensitive part of the reaction that determines the diameter of formed particles [35].

The diameter of the PS-NR particles can be modified by changing the PVP concentration during the polymerisation. Lowering the PVP concentration led to an increase of the average diameter (table 1, samples PS-NR-2, PS-NR-3, PS-NR-4). Images of the particles are shown in SM-figure 1. Figure 3(a) shows that the diameter of PS-NR particles decreased approximately linearly with the increase of PVP concentration in the investigated concentration range.

In one preparation, the volume ratio EtOH:H_2O was changed to 20:80 (PS-NR-5, table 1). As a result, highly polydisperse spherical particles with diameters ranging from few hundred nm up to 50 μm were obtained (see figures 2(g) and (h)). Some polymeric lumps were also observed on the walls and reactor bottom. The presence of large microspheres and polymeric lumps suggests a high reaction rate in an unstable system with larger heterogeneity caused by the increased water/PVP ratio (table 1). Remarkably, the formed particles still kept their spherical morphology thus enabling the preparation of high molecular weight PS-NR microspheres with a wide range of sizes.

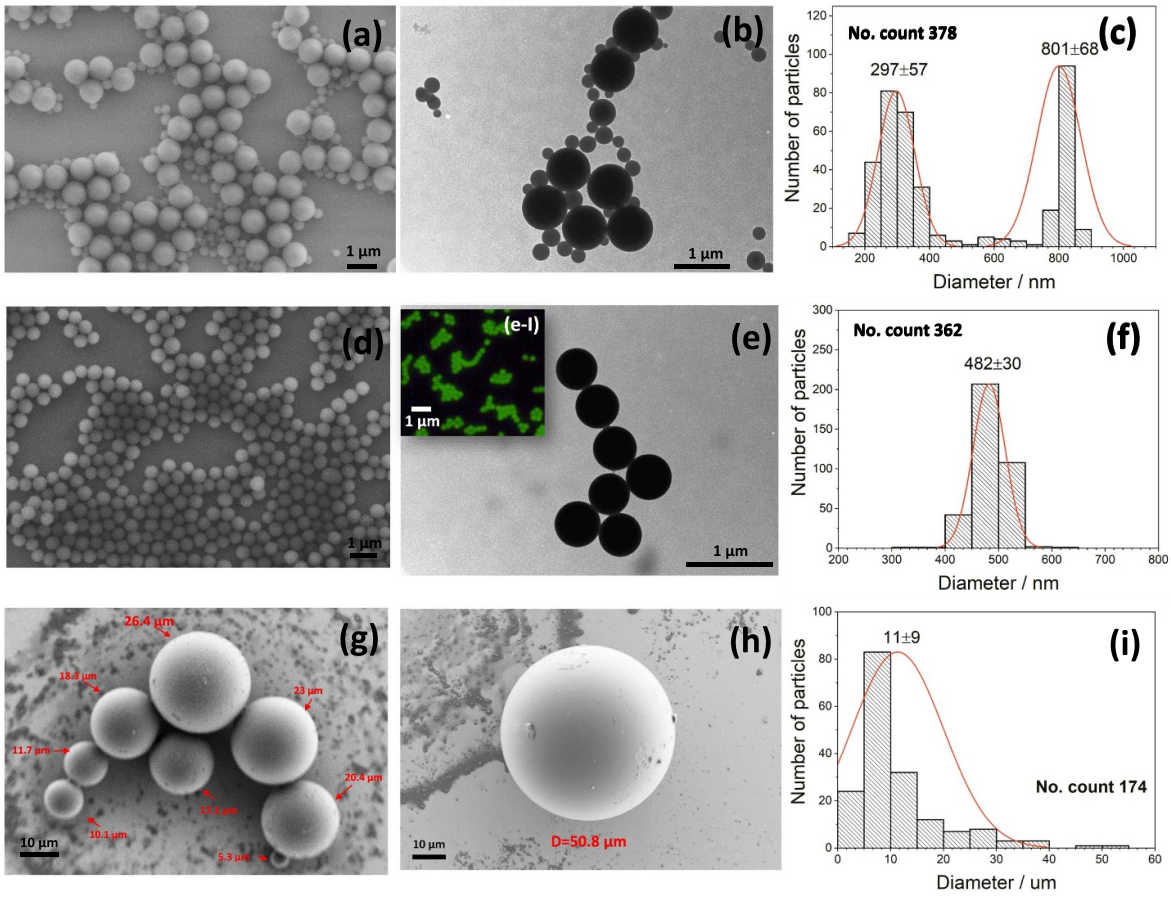

Figure 2. Particles by MW-assisted polymerisation; PS-0 (top row, (a)–(c)), PS-NR-1 (middle row, (d)–(f)), PS-NR-5 (bottom row, (g)–(i)): (a), (d), (g), (h) SEM images, (b), (e) TEM images and (c), (f), (i) histograms of diameter distribution. Inset (e-I): fluorescence microscopy image of PS-NR-1. Red label numbers (g), (h) correspond to diameter of the microspheres for the larger particles.

Table 1. Diameter of PS particles obtained using different reaction conditions by dispersion polymerisation. PVP: poly-(N-vinyl pyrrolidone) concentration. Polymerisation time: 2 h.

Sample	Heating	PVP g/g styrene	EtOH/H_2O vol. ratio	dye conc. μg NR/g styrene	$\langle D \rangle$ nm
PS-0	MW	10%	80:20	0	800 ± 70[a]
					300 ± 60[a]
PS-NR-1	MW	10%	80:20	187	480 ± 30
PS-NR-2	MW	7.5%	80:20	187	780 ± 20
PS-NR-3	MW	5%	80:20	187	1030 ± 40
PS-NR-4	MW	2.5%	80:20	187	1190 ± 50[a]
					1540 ± 160[a]
PS-NR-5	MW	10%	20:80	187	Polydisperse[b]
PS-NR-6	CH	10%	80:20	187	440 ± 30
					330 ± 30

[a] Bimodal size distribution.
[b] PS particles ranging from hundreds of nanometers up to 50 μm were obtained (SM-figure 3).

Finally, the reaction medium composition of PS-NR-1 was used in a synthesis with an electric mantle as heater instead of MW irradiation ('conventional heating'; sample PS-NR-6, table 1). PS-NR particles with well defined spherical morphology, slightly smaller diameter and broader diameter distribution than with MW heating were obtained (table 1, SM-figure 3).

To further explore the PS-NR particle preparation process, the fraction of converted monomer, mean particle diameter and diameter distribution of the PS-NR particles in different

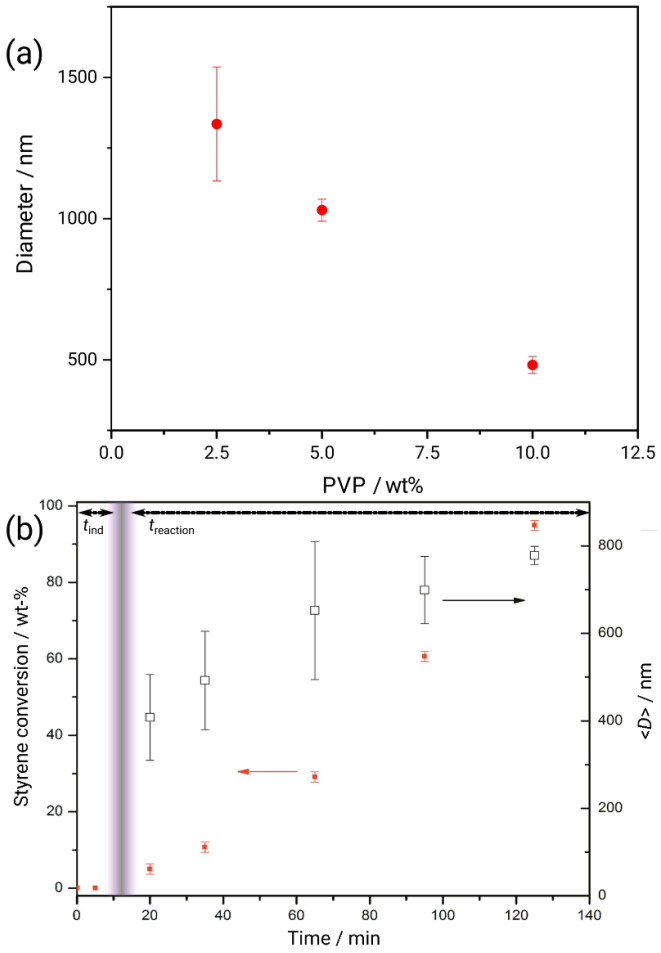

Figure 3. (a) Effect of PVP amount (number denotes mass PVP per mass monomer in %) on diameter and diameter distribution, FWHM indicated by the error bar, of PS-NR particles. (b) Kinetics of styrene conversion and PS-NR particles mean diameter $\langle D \rangle$ as obtained from histogram analysis of SEM images at different stages of free radical *in situ* dye doping polymerisation using MW activation; conditions: 200 W MW, EtOH:H_2O ratio 80:20 (v/v), 7.5 wt.-% PVP.

stages of the MW-assisted polymerisation were investigated by gravimetric and SEM analyses.

Figure 3(b) shows the styrene conversion and the PS-NR diameter evolution with reaction time. In the curve of styrene conversion, two main reaction time phases can be distinguished. The first phase corresponds to the induction time t_{ind}, where the MW absorption leads to an increase in temperature of the reaction medium until the reaction temperature 80 °C was reached. Using 200 W of constant MW irradiation, $t_{ind} \approx 5$ min was needed to reach the boiling point of reaction medium (80:20 vol% of ethanol–water mixture) and to start the free radical polymerisation reaction by the thermal decomposition of AIBN. The second phase is the reaction phase, where the styrene conversion continuously increased. After 2 h of MW irradiation, more than 94% of styrene was polymerised.

Figure 3 and SM-figure 3 show the mean particle diameter, the SEM images and the diameter histograms of PS-NR particles at different stages of the polymerisation. PS-NR particles with well defined morphology, high diameter polydispersity ranging from 230 to 750 nm as well as $\langle D \rangle = (410 \pm 100)$ nm and $\langle D \rangle = (490 \pm 110)$ nm were produced during the first 15 min and 30 min, respectively, of MW assisted polymerisation (SM-figures 3(a) and (b)). The diameter distribution became narrow after 90 min of MW irradiation, when spheres with $\langle D \rangle = (699 \pm 77)$ nm were produced (SM-figure 3(d)). Uniform PS-NR particles with $\langle D \rangle = (780 \pm 20)$ nm and thus a narrower diameter distribution were finally obtained after 2 h of reaction time (SM-figure 1(a)). Incorporation of NR was proven by UV–VIS spectroscopy (SM section 4).

The particle growth can be explained using the dispersion polymerisation process reported in the literature [42, 43]. The key step in this suggested formation mechanism is the rapid heating by MW irradiation that produces initially many nuclei where polymerisation-trapping of styrene-NR can occur. This mechanism can explain the high polydispersity of the particles during the early stage of the polymerisation. At longer MW irradiation duration, the free styrene and NR still contained in the continuous phase are then absorbed into the unstable smaller particles. These monomer-dye swollen particles are subsequently polymerised while their diameter increases. Figure 4 shows a schematic representation of PS-NR growth during the MW-assisted polymerisation.

PS-NR microsphere syntheses reported in literature used (i) the copolymerisation reaction of an allyl NR precursor with styrene by conventional heating up to a reaction time of 48 h [53], or (ii) the dye doping of preformed PS microspheres by a swelling procedure [54]. While the first process involved several steps, including the preparation of the allyl NR precursor and long reaction time, the second approach was less time consuming but is limited to the PS microspheres available on the market. The single step procedure here reported is therefore an attractive alternative as it is fast and convenient.

2.2. *Evaluation of PS-NR microspheres as WGM-μRs*

A typical series of WGM spectra in air for individual PS-NR microspheres with diameters from 3.5 to 15 μm are shown in figure 5. Optical response was assessed at pump power values from 0.1 to 12.2 μW. It is observed that the intensity of the modes for all particles increases with the pump power. The onset of WGM excitation was at ≈0.2 μW for particles of $D > 7$ μm, and 0.7 μW for the smallest evaluated particle of $D \approx 3.5$ μm.

Overall, particles ranging from ≈1 to ≈30 μm were tested as WGMs resonators. The particle selection was carried out arbitrarily. The smallest particle to support WGMs had a diameter of ≈3.5 μm. It was more challenging to excite WGMs in particles with a diameter $\lesssim 5$ μm in comparison to larger particles. In this size range, approximately every second tested particle showed WGMs. For larger particles with $D \gtrsim 5$ μm, it was straightforward to excite WGMs. However, as expected, particles with visible imperfections did not support WGMs. Every tested particle free of imperfections showed WGMs.

The very low pumping power required to excite WGMs in *in situ* doped resonators can be a consequence of a more effective entrapment and thus higher gain of the dye inside

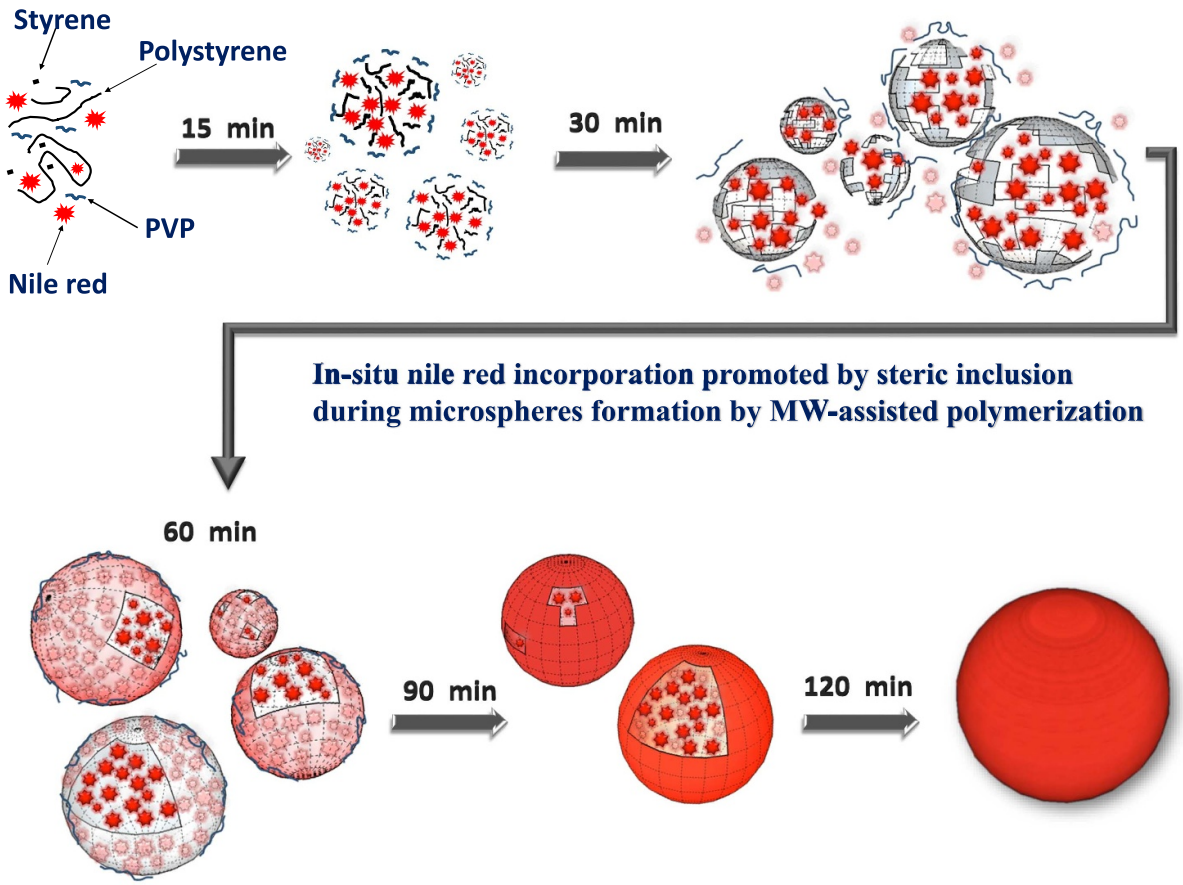

Figure 4. Scheme showing NR incorporation during the PS particle growth in MW-assisted free radical *in situ* dye doping polymerisation.

the particles. Here, the distribution of the dye in the spheres is expected to be uniform along the whole volume of the particles as the dye is not diffusing into the spheres after the synthesis but into the growing particles throughout the preparation process. Thus, one expects increasing dye quantum efficiency compared to particles with *ex situ* dye incorporation [21]. Possible composition gradients provoked by diffusion limitations during the doping approach by the soaking are in this manner circumvented. It is also evident that the density of modes per spectrum decreases along with decreasing D of the PS particle, as the axial mode spacing, the 'free spectral range' (*FSR*) of an optical resonator increases with the decreasing sphere diameter [11], as will be quantitatively evaluated below.

Q and FWHM were determined from spectra at different pump powers for microspheres with $D < 10\ \mu$m and are shown in figure 6. Overall, $Q = \mathcal{O}(10^2 \ldots 10^3)$ were found. The uncertainties were obtained from the standard error propagation of the Gaussian peak fitting. As Q describes the stored energy in the resonator, it is not surprising that particles with larger diameter exhibit higher Q. Q increases with increasing pump power, mainly through a decrease in FWHM. However, resonators operated at low Q are expected to give a larger spectral shift of the mode position when changing the surrounding medium [12]. In a similar system, lasing was observed for spheres with $D \approx 10\ \mu$m, at similar orders of magnitude of Q [21].

Figure 7 shows WGMs measurements carried out in air and water to probe refractive index sensing of microsphere resonators with a D in the range 5–30 μm. The pump power used for air and water measurements was set to 12.2 and 42.3 μW, respectively. For these particles in air, the *FSR* was determined from experimentally observed peaks in air (table 2). Further, *FSR* was calculated showing good agreement in most cases. A slight mismatch was found between experimental and theoretical value for the 10 μm microsphere, possibly caused by heating in polymer microspheres with high surface roughness. Such heating effects may lead to lower *FSR* than the theoretically expected value [55].

In comparison with air, a higher excitation power is needed to excite WGMs in water, in line with other observations [21]. The maximum permissible power in water before the particles get damaged was 227 μW; testing the next step of our pump source (377 μW) resulted in a completely burned particles.

The evaluation of the particles as sensors for the surrounding refractive index was carried out by measuring WGM spectra in air and in water. The mode calculation (details see SM-section 1.3.6) was done for the four microresonators shown in figure 7, using the assumption of a homogeneous sphere in a medium with known refractive index. Results of the analysis are summarised in table 2. Deviations between the diameters may be caused by the approximation in the simulation of the WGM spectra. The pattern of the spectra in both air

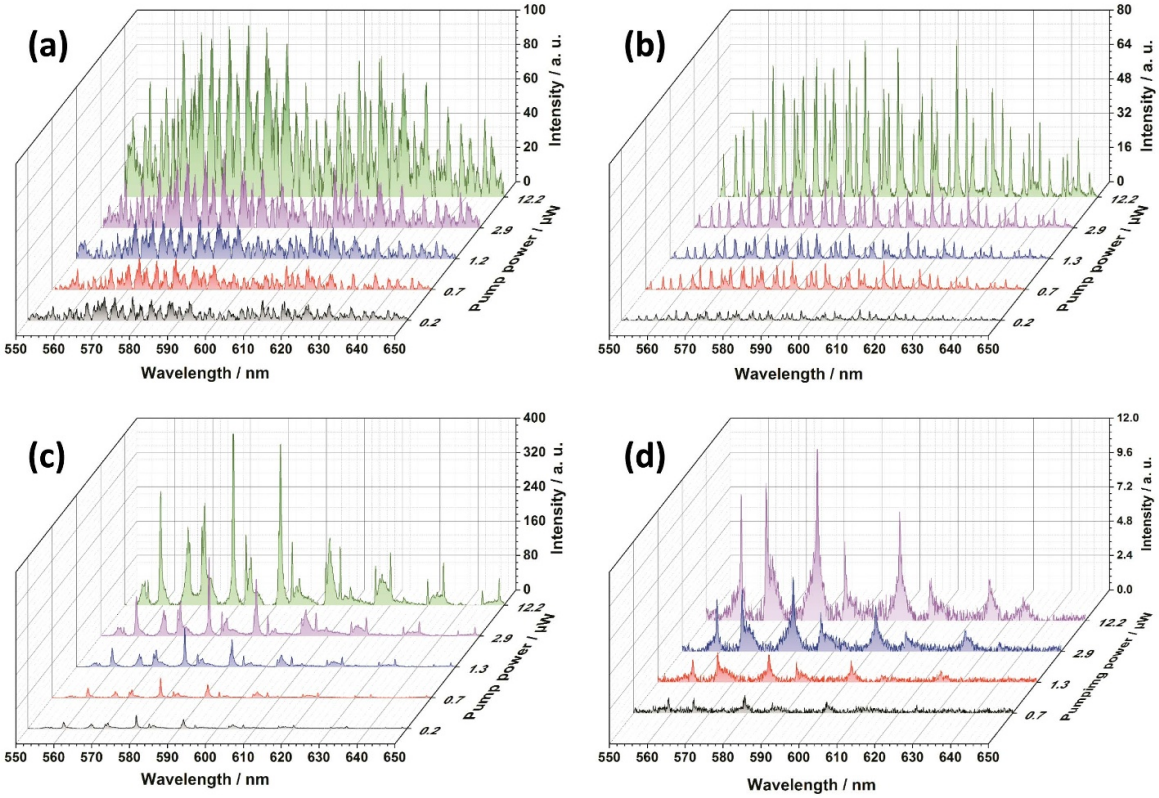

Figure 5. WGM spectra (excitation wavelength 532 nm) after subtraction of fluorescence background obtained in air from PS-NR microspheres with $D \approx (15 \pm 0.5)$ μm (a), (9.2 ± 0.2) μm (b), (7 ± 0.1) μm (c), and (3.5 ± 0.1) μm (d), with increasing pump power (0.1–12.2 μW). The uncertainty estimate comes from the precision of the microscopic diameter determination.

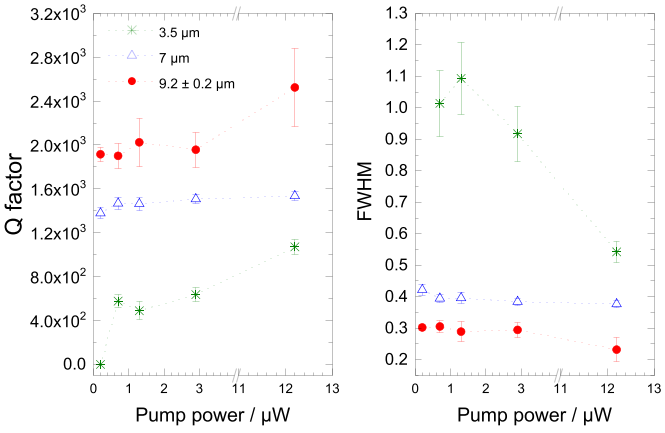

Figure 6. Q (left) and FWHM (right) as function of pump power for particles with $D \approx (9.2 \pm 0.2)$ μm, (7 ± 0.1) μm, and (3.5 ± 0.1) μm.

and water were very similar except for the smallest investigated sphere, with slight variation in the intensity of WGMs for the chosen polymer microsphere. However, a wavelength shift in the WGMs can be observed when changing the surrounding medium from air to water. It has to be noted that the WGM spectra of polymer microspheres recorded in water has a very low intensity as compared to measurement in air. To obtain intense WGMs, a higher pumping power of the laser was used when measurement was carried out in water. Hence, the pattern of the two spectra were similar—with differences in the details—even though the experimental conditions are quite different within the recorded spectral range. The shifts in resonance wavelengths for different spectra varies because of the variation in the free spectral range. Comparative plots for the experimentally observed and analytically calculated mode numbers are shown in SM-figure 5 for all four microspheres analysed in table 2.

In figure 7, the shift for the smallest particle is obvious, whereas for the bigger particles, it is intuitively hard to understand that intensity ratios between different peaks depends on the wavelengths, not on mode number. For example, in figure 7(c), the two peaks at the lower wavelengths wave similar intensity ratio in water and in air, though they do not belong to the same modes assuming that the mode assignment is correct. In figure 7(a), even minor details of the spectra seem to agree, so that one could reason there is no effect of the surrounding medium on the spectrum at all for the 30 μm microresonator. We hypothesise here that either (1) the internal structure of the particle or (2) micromorphological features on the particle surface are responsible for the similarities.

If (1) the internal structure would show a distribution gradient of e.g. the dye or polymer such that there is a refractive index gradient from higher (inside) to lower (outside)

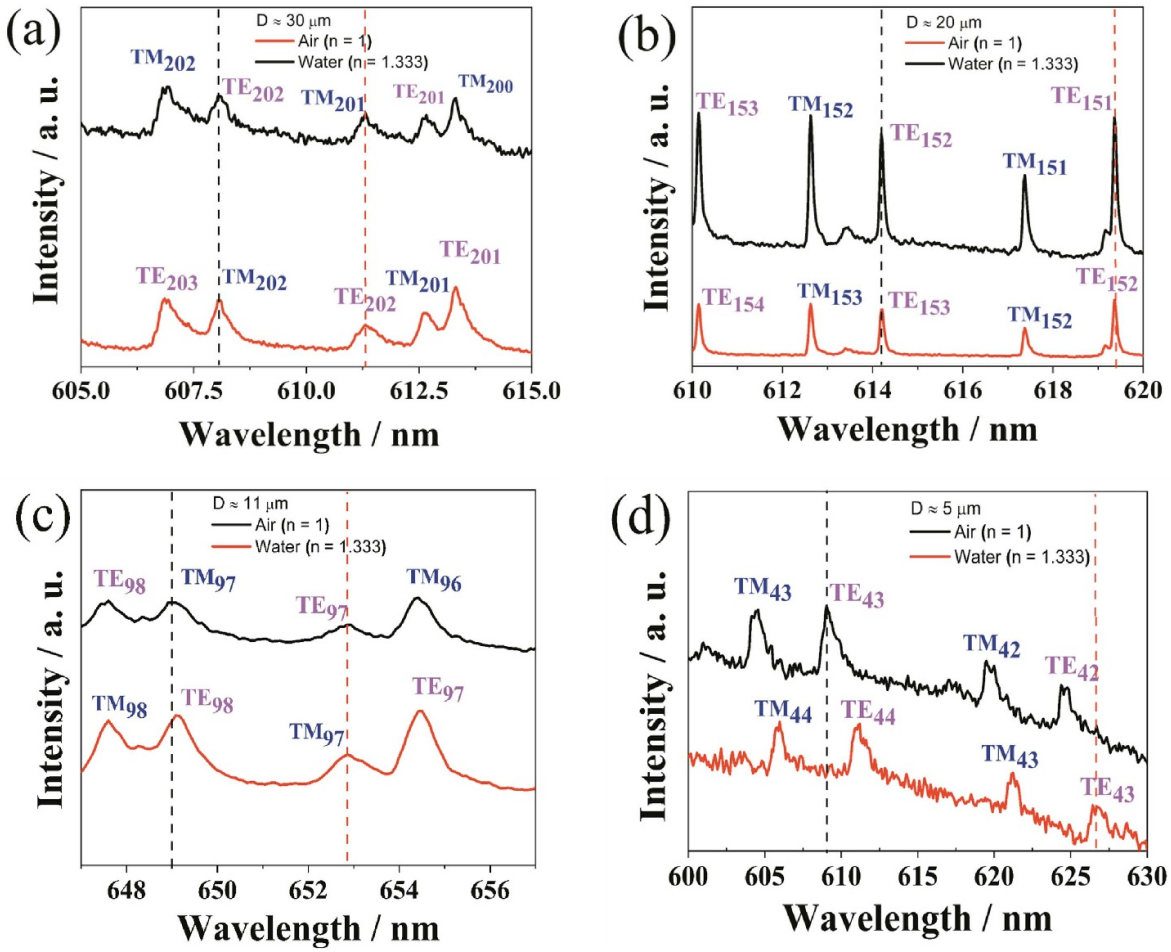

Figure 7. WGMs spectra obtained from particles with different diameter in air (refractive index of surrounding medium $n_e = 1$) and water ($n_e = 1.333$): (30 ± 0.8) μm (a), (20 ± 0.6) μm (b), (11 ± 0.3) μm (c), and (5 ± 0.2) μm (d). (a, b) recorded with grating of 1800 mm^{-1}, (c, d) with grating of 600 mm^{-1}. Quantitative analysis in table 2.

Table 2. Experimental and calculated free spectral range in air, $FSR_{(calc.)} = \lambda^2/(n\pi D)$. Mode shifts when changing surrounding medium from air to water from spectra in figure 7 analysed for selected particles. D_{Micr}—microscopic diameter; D_{WGM}—diameter from WGM analysis; $\delta\lambda_{max}$—maximum observed mode shift, for indicated mode; $\delta\lambda_{ave}$—average observed mode shift; S calculated with equation (2).

D_{Micr} μm	D_{WGM} μm	$FSR_{(exp.)}$ nm	$FSR_{(calc.)}$ nm	$\delta\lambda_{max}$ nm	f. mode	$\delta\lambda_{ave}$ nm	S nm/RIU
5	6	13.7	14.0	17.4	TE43	13.9	53
11	13.8	5.4	7.6	3.8	TM97	2.5	11
20	20	3.6	3.7	5.2	TE152	4.0	16
30	26	2.0	2.5	3.1	TE202	1.5	9

refractive index, the modes in the particles may actually not interact as strongly with the outside medium as one would assume for the homogeneous sphere. Importantly, PS particles are radially birefringent [56], which also affects the interaction with the surrounding medium. If the internal field distribution is affected by the internal structure of the particle, the presented mode assignment may be wrong as the prerequisites for using the theory may not be fulfilled. A further effect may arise (2) from micromophological features, such as surface defects. These defects will lead to scattering and thus peak broadening. Due to the fact that for the same particle in two media, the surface defects will be located at fixed positions relative to each other, coherent interaction with these defects could possibly affect certain specific wavelengths more than others. Possibly, such effects may lead to peak broadening becoming strongly wavelength dependent, so that the resulting broadening is more wavelength-specific than mode-specific.

The maximum peak shift with change in medium was observed for the smallest particle. Against expectations, it was observed that mode shifting increased from 30 to 20 μm microspheres but again it decreased for 11 μm. This change arises from the very small FWHM for the 11 μm resonator in comparison to the 20 μm particle. The maximum sensitivity of 52 nm/RIU is calculated for a 5 μm WGM-μR. It must be

stressed that all measurements were conducted on individual particles, so that differences between those particles may screen overarching trends. A possible reason for deviations from overarching trends is thus e.g. a slight deviation from a perfect spherical shape from the individual studied particle. Another possible reason for deviation is surface roughness or the presence of individual surface defects on the μRs [57, 58]. With increasing diameter and thus increasing surface area, the probability of the presence of defects increase, as do possible effects of the surface roughness. The trend of increasing roughness may overshadow other trends, e.g. the expected increase in Q with increasing diameter.

3. Conclusions

PS-based, laser dye doped WGM-μRs were prepared in a single step, time efficient MW-assisted polymerisation process. The direct dye incorporation by MW-assisted polymerisation avoids tedious multistep doping using e.g. in-diffusion of dye, which may result in concentration gradients in the μRs. The heterophase polymerisation protocol also minimises the use organic solvents. The particles are spherical, and their diameter and diameter distribution were easily controlled by modifying the stabiliser concentration and the ethanol:water ratio. The MW-assisted polymerisation process using the dipole coaxial antenna owns versatility, fast processing times and high yields. The setup integrates well with standard laboratory glassware or larger scale industrial reactors, and is easily scalable. Importantly, depending on processing parameters, either very high polydispersity or monodisperse particles can be prepared.

The obtained microspheres with $D \gtrsim 3.5$ μm supported WGMs which could be coupled through space by exciting the fluorescence of the laser dye NR, in both air an aqueous solutions. The sensitivity of WGMs towards change in the refractive index was on the order of 50 nm/RIU, comparable or even slightly higher than observed for other polymer-based resonators before. As expected, the smallest particles supporting WGMs showed the highest sensitivity towards refractive index sensing, on the expense of the quality factor, which is on the order of 10^3. The diameter of this particle is lower than other PS particles reported in the literature known to us to support WGMs in water. The main drawback at the moment appears to be the stability of the system. While higher sensitivity and stability can be reached with high refractive index materials such as oxides, standard PS colloid chemistry offers the possibility to make the particles biocompatible or to incorporate further aspects. The combination of low excitation energy and high sensitivity for this class of particles opens new perspectives for such polymer particles for enhanced biosensing applications.

Data availability statement

The data that support the findings of this study are available upon reasonable request from the authors.

Acknowledgments

J S M O thanks the Mexican Consejo Nacional de Ciencia y Tecnología (CONACYT) for a scholarship. We thank Petra Ebbinghaus for technical assistance.

Author contributions

J M-O, J G-R: investigation, formal analysis, writing—original draft; C T, R K: investigation, formal analysis; R S M, C D, C F, G B: Resources, Supervision, Writing—review and editing; A E: conceptualisation, methodology, resources, supervision, writing—reviewing and editing.

ORCID iDs

Rakesh S Moirangthem https://orcid.org/0000-0002-5628-0115
Giuseppe Barillaro https://orcid.org/0000-0001-6197-4851
Andreas Erbe https://orcid.org/0000-0002-8865-0256

References

[1] Liao J and Yang L 2021 *Light: Sci. Appl.* **10** 32
[2] Hao Y and Guo Z 2019 *J. Phys. D: Appl. Phys.* **52** 175101
[3] Mehrabani S, Kwong P, Gupta M and Armani A M 2013 *Appl. Phys. Lett.* **102** 241101
[4] Ali A R and Kamel M A 2017 *Math. Probl. Eng.* **2017** 9649524
[5] Ali A R and Ioppolo T 2014 *Sensors* **14** 7041–8
[6] Jin W L, Yi X, Hu Y W, Li B B and Xiao Y F 2013 *Appl. Opt.* **52** 155–61
[7] Reynolds T, Riesen N, Meldrum A, Fan X, Hall J M M, Monro T M and François A 2017 *Laser Photonics Rev.* **11** 1600265
[8] Kuwata-Gonokami M and Takeda K 1998 *Opt. Mater.* **9** 12–17
[9] Moirangthem R S and Erbe A 2013 *Appl. Phys. Lett.* **103** 051108
[10] François A, Rowland K J and Monro T M 2011 *Appl. Phys. Lett.* **99** 141111
[11] Francois A and Himmelhaus M 2009 *Sensors* **9** 6836–52
[12] Vollmer F and Arnold S 2008 *Nat. Methods* **5** 591–6
[13] Ta V D, Chen R and Sun H D 2013 *Sci. Rep.* **3** 1362
[14] Paunoiu A, Moirangthem R S and Erbe A 2015 *Phys. Status Solidi* **9** 241–4
[15] Fabitha K, Wakiyama Y, Oshima H, Nakamura D and Rao M S R 2020 *J. Phys. D: Appl. Phys.* **53** 135302
[16] Ma K, Zhou X, Kan C, Xu J and Jiang M 2021 *Phys. Chem. Chem. Phys.* **23** 6438–47
[17] Cai L, Pan J, Zhao Y, Wang J and Xiao S 2020 *Phys. Status Solidi* a **217** 1900825
[18] Zhi Y, Yu X C, Gong Q, Yang L and Xiao Y F 2017 *Adv. Mater.* **29** 1604920
[19] Okada D *et al* 2020 *Mater. Horiz.* **7** 1801–8
[20] Foreman M R, Swaim J D and Vollmer F 2015 *Adv. Opt. Photonics* **7** 168–240
[21] François A, Riesen N, Ji H, Afshar V S and Monro T M 2015 *Appl. Phys. Lett.* **106** 031104
[22] Toropov N, Cabello G, Serrano M P, Gutha R R, Rafti M and Vollmer F 2021 *Light: Sci. Appl.* **10** 42
[23] Kelemen L, Lepera E, Horváth B, Ormos P, Osellame R and Martínez Vázquez R 2019 *Lab Chip* **19** 1985–90

[24] François A, Riesen N, Gardner K, Monro T M and Meldrum A 2016 *Opt. Express* **24** 12466–77
[25] Li H, Hao X, Li Y, Duan R, Zhang T, Li J, Yuan Y and Liu L 2021 *J. Mater. Sci.* **56** 570–80
[26] Monguzzi A, Frigoli M, Larpent C and Meinardi F 2012 *RSC Adv.* **2** 11731–6
[27] Vollmer F, Braun D, Libchaber A, Khoshsima M, Teraoka I and Arnold S 2002 *Appl. Phys. Lett.* **80** 4057–9
[28] White I M, Oveys H and Fan X 2006 *Opt. Lett.* **31** 1319–21
[29] Septiadi D, Barna V, Saxena D, Sapienza R, Genovese D and De Cola L 2020 *Adv. Opt. Mater.* **8** 1901573
[30] Nguyen T T, Mai H H, Pham T V, Nguyen T X and Ta V D 2021 *J. Phys. D: Appl. Phys.* **54** 255108
[31] Nguyen T V, Mai H H, Nguyen T V, Duong D C and Ta V D 2020 *J. Phys. D: Appl. Phys.* **53** 445104
[32] Lv Y *et al* 2020 *Nano Lett.* **20** 2020–5
[33] Chen X, Xie K, Hu T, Zhang X, Yang Y, Ma J, Zhang J, Cheng X and Hu Z 2019 *J. Phys. D: Appl. Phys.* **52** 475104
[34] Cheeney J E, Hsieh S T, Myung N V and Haberer E D 2020 *Nanoscale* **12** 9873–83
[35] Peng G, Wang B, Meng X, Liu B and Luo R 2015 *J. Appl. Polym. Sci.* **132** 41927
[36] Zhao X, Zhou S, Chen M, Wu L and Gu G 2011 *J. Appl. Polym. Sci.* **119** 3615–22
[37] Kempe K, Becer C R and Schubert U S 2011 *Macromolecules* **44** 5825–42
[38] Brooks W L A and Sumerlin B S 2012 *Isr. J. Chem.* **52** 256–63
[39] Zhou Y N, Li J J, Wu Y Y and Luo Z H 2020 *Chem. Rev.* **120** 2950–3048
[40] Sinnwell S and Ritter H 2007 *Aust. J. Chem.* **60** 729–43
[41] Lidström P, Tierney J, Wathey B and Westman J 2001 *Tetrahedron* **57** 9225–83
[42] Xu Z S, Deng Z W, Hu X X, Li L and Yi C F 2005 *J. Polym. Sci.* A **43** 2368–76
[43] Zhu M Q, Chen G C, Li Y M, Fan J B, Zhu M F and Tang Z 2011 *Nanoscale* **3** 4608–12
[44] Das G *et al* 2017 *J. Am. Chem. Soc.* **139** 9558–65
[45] Li G, Yu K, Noordijk J, Meeusen-Wierts M H M, Gebben B, Oude Lohuis P A M, Schotman A H M and Bernaerts K V 2020 *Chem. Commun.* **56** 9194–7
[46] Martín-Illán J A, Rodríguez-San-Miguel D, Franco C, Imaz I, Maspoch D, Puigmartí-Luis J and Zamora F 2020 *Chem. Commun.* **56** 6704–7
[47] González-Rivera J, Galindo-Esquivel I R, Onor M, Bramanti E, Longo I and Ferrari C 2014 *Green Chem.* **16** 1417–25
[48] González-Rivera J, Duce C, Ierardi V, Longo I, Spepi A, Tiné M R and Ferrari C 2017 *ChemistrySelect* **2** 2131–8
[49] Spepi A, Duce C, Ferrari C, González-Rivera J, Jagličić Z, Domenici V, Pineider F and Tiné M R 2016 *RSC Adv.* **6** 104366–74
[50] González-Rivera J, Tovar-Rodríguez J, Bramanti E, Duce C, Longo I, Fratini E, Galindo-Esquivel I R and Ferrari C 2014 *J. Mater. Chem.* A **2** 7020–33
[51] Zhang X, Shen S and Fan L 2008 *Polym. Bull.* **61** 19–26
[52] Qi H, Hao W, Xu H, Zhang J and Wang T 2009 *Colloid Polym. Sci.* **287** 243–8
[53] Liu Q H, Liu J, Guo J C, Yan X L, Wang D H, Chen L, Yan F Y and Chen L G 2009 *J. Mater. Chem.* **19** 2018–25
[54] Behnke T, Würth C, Hoffmann K, Hübner M, Panne U and Resch-Genger U 2011 *J. Fluoresc.* **21** 937–44
[55] Liu Z *et al* 2016 *Opt. Lett.* **41** 4649–52
[56] Erbe A, Tauer K and Sigel R 2009 *Langmuir* **25** 2703–10
[57] Chien C H, Khanum R, Liu C L, Moirangthem R S and Chang Y C 2021 *Opt. Mater. Express* **11** 1568–74
[58] Henriet R, Lin G, Coillet A, Jacquot M, Furfaro L, Larger L and Chembo Y K 2015 *Opt. Lett.* **40** 1567–70